Calibration of the Johnson-Cook Material Model for Additively Manufactured 304L SS Parts: Modeling and Experiments

M. Rangapuram[1], S. K. Dasari[1], S.P. Isanaka[1], M.F. Buchely[2], J. W. Newkirk[2] and K. Chandrashekhara[1]

[1]Department of Mechanical and Aerospace Engineering
[2]Department of Materials Science and Engineering
Missouri University of Science and Technology, Rolla, MO 65409

Abstract:

Selective laser melting (SLM) is a type of additive manufacturing technique which uses a powder bed to form complex metal parts in a layer-by-layer process. This study aims to understand the material flow of parts manufactured by SLM process using 304L stainless steel powder, which is widely used in numerous applications. The tensile specimens were manufactured using 304LSS powder through SLM process. Low strain-rates, high temperature tensile tests were carried out to calibrate the parameters of the constitutive Johnson-Cook strength model. To conduct the tensile tests, different temperatures (25 ºC, 150 ºC and 250 ºC) and strain-rates (0.1 s^{-1}, 0.01 s^{-1} and 0.001 s^{-1}) were used. The material model developed was used in numerical simulation of the tensile tests and compared with the experimental results.

1. Introduction

Owing to its design flexibility, dexterity, and reduced material loss additive manufacturing (AM) is gaining a lot of importance in recent times [1]. Laser Powder Bed Fusion (LPBF) is a type of additive manufacturing process in which a uniform powder bed resulting from a spreading process interacts with a laser source to irradiate the powder in a sequential layer process. LPBF is typically used manufacturing complex structures [2]. Historically researchers investigated the influence of build parameters on the manufactured part [3-5]. Apart from the process parameters itself the quality and the properties of the printed part also depend on the type of material, the conditions used for manufacturing, machine and methodology used in the printing process. The rapid melting, solidification of the powder involves complex physical phenomena happening at the same time [6]. The rapid cooling rates which are quite inherent with the process result in non-equilibrium phases and influences the microstructure of the material. This is the reason for the difference in the properties and behavior from the conventionally manufactured counterparts [7].

Some of the prominent works by researchers in characterizing the material as well as material behavior of through AM is reported below. The process parameters in the AM affects the anisotropy and mechanical properties. Optimizing these process parameters can improve the performance of the manufactured part. Popovich et al. [8] studied the relationship between the build orientation and the mechanical properties of the Ti6Al4V. Miranda et al. [9] assessed the properties of 316L stainless steel using a predictive model. Ortiz et al. [10] investigated the tensile properties of 304L stainless steel varying the orientation, part thickness and the build size. Guan et al. [11] studied the mechanical properties using different hatch angles.

Optimizing the parameters solely based on experimental effort can be time consuming and costly. There is a need to use the computational effort to develop models that optimize the process parameters and predict the properties [12]. Zhang et al. [13] used a thermal model to study the laser power and scan speed effects on the melt pool. Due to the dynamic non-homogeneity of the AM processed parts the tensile and the yield strength were four times and two times higher than the as-cast material [14]. The study that involves the plastic deformation of any material will be specific to the material and the experimental effort may take a long time. This can be studied using Finite Element (FE) models. Segebade et al. [15] studied the anisotropic deformation characteristics of AlSi10Mg. The deformation mechanisms in biocompatible Ti6Al4V were investigated by Kadkhodapour et al. [16]. Their study revealed that the use of Johnson-Cook damage model can estimate the stresses within 18% error. There is very limited to no data on the JC parameters for additively manufactured steels. The material used in this study is 304L stainless steel.

304L stainless steel has gained importance over the years due to its mechanical properties and chemical compositions. LPBF of 304L stainless steel to fabricate parts does not require any post processing like solution annealing due to low carbon content which reduces the precipitation of carbide [17]. 304L stainless steel manufactured through AM results in superior mechanical (tensile and yield strength) than conventionally manufactured counterparts. This makes them a perfect candidate for high strength applications [18].

Johnson-Cook (JC) model is a widely used analytical model to predict the material flow at different temperatures and strain-rates [19]. The JC model deals with the relationship affecting the stress with strain, strain rate and the temperature. The yield stress in JC models is given by the equation below:

$$\sigma_0 = [A + B\varepsilon^n]\left[1 + Cln\left(\frac{\dot{\varepsilon}}{\dot{\varepsilon_0}}\right)\right][1 - (T^*)^m] \quad (1)$$

where $[A + B\varepsilon^n]$ is the stress term expressed as a function of strain, $[1 + Cln\left(\frac{\dot{\varepsilon}}{\dot{\varepsilon_0}}\right)]$ captures the strain rate effect, $[1 - (T^*)^m]$ captures thermal effects, where T^* can be expressed as:

$$T^* = \frac{T - T_r}{T_m - T_r} \quad (2)$$

T_r is the reference temperature, T_m is the melting temperature.

In this work, an effort was made to develop the constitutive JC model for additively manufactured 304L stainless steel. Low strain-rates tensile tests were performed at various temperatures and strain-rates to obtain these material parameters. These obtained parameters were used in developing an FE model to simulate the tensile behavior of the AM material. The accuracy of the developed model was compared to the actual tensile testing experiments.

2. Materials and methods

2.1 Manufacturing of 304L SS with LBPF

The tensile specimens were manufactured using gas atomized 304L stainless steel powder with a particle size ranging from 15 µm to 63 µm. The chemical composition (wt%) of the material can be found in Table 1. The fabrication of the 304L SS parts was carried out using Renishaw AM250 machine. The machine process parameters used in this study are listed below (Table 2).

Table 1. Chemical composition of 304L stainless steel powder

Fe	C	N	Si	Ni	Cr	Mn	Cu	Mo	P
69.9	0.025	0.07	0.015	7.9	17.7	1.75	0.84	0.32	0.03

Table 2. Machine parameters of Renishaw AM250

Process parameter	Value
Effective build volume (mm x mm x mm)	248 x 248 x 280
Laser power (W)	200
Laser type	1070 nm NdYAG
Laser spot	70
Hatch distance (mm)	0.085
Layer thickness (µm)	50
Point distance (µm)	60
Exposure time (µs)	75
Point distance (µm)	60
Inert gas during production	Argon

2.2 Manufacturing of tensile coupons

The Renishaw AM250 machine was used to manufacture the tensile coupons for this study. ASTM-E8 subsize specimens were printed in both XY and Z directions. The ASTM-E8 specimen with the dimensions can be found in Figure 1. The specimen was 2 mm thick with a 2º taper included in the design to induce the failure in gauge section of the specimen.

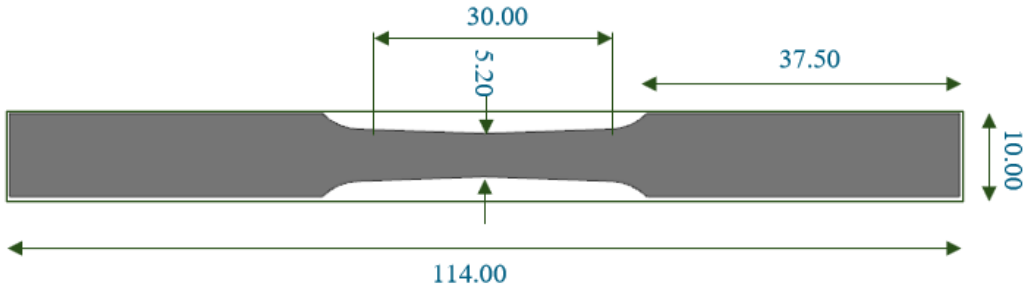

Figure 1. ASTM-E8 subsize specimen (dimensions in mm)

3. Low strain-rates tensile testing

The JC model was used to investigate the plastic deformation of 304L stainless steel in this work. To obtain the JC parameters of the material, low strain-rate tensile tests were performed at various temperatures and strain rates. The temperatures of 25ºC, 150ºC, 250ºC and the strain rates of 0.1 s^{-1}, 0.01 s^{-1}, 0.001 s^{-1} were chosen for this work. These ranges were mainly selected with respect to the structural application of the material. The complete experimental test matrix can be found in Table 3. Five replications were performed for each combination of temperature and strain rate.

Table 3. Experimental test matrix

Strain rate	**Temperature**		
	25 ºC	**150 ºC**	**250 ºC**
0.1 s^{-1}	(0.1,25)	(0.1,150)	(0.1, 250)
0.01 s^{-1}	(0.01, 25)	(0.01, 150)	(0.01, 250)
0.001 s^{-1}	(0.001, 25)	(0.001, 25)	(0.001, 250)

3.1 Testing

The tensile tests were performed on an MTS frame with environmental chamber to control the temperature. The MTS machine (Figure 2a) and the specimen installed in the environmental chamber can be found in Figure 2b.

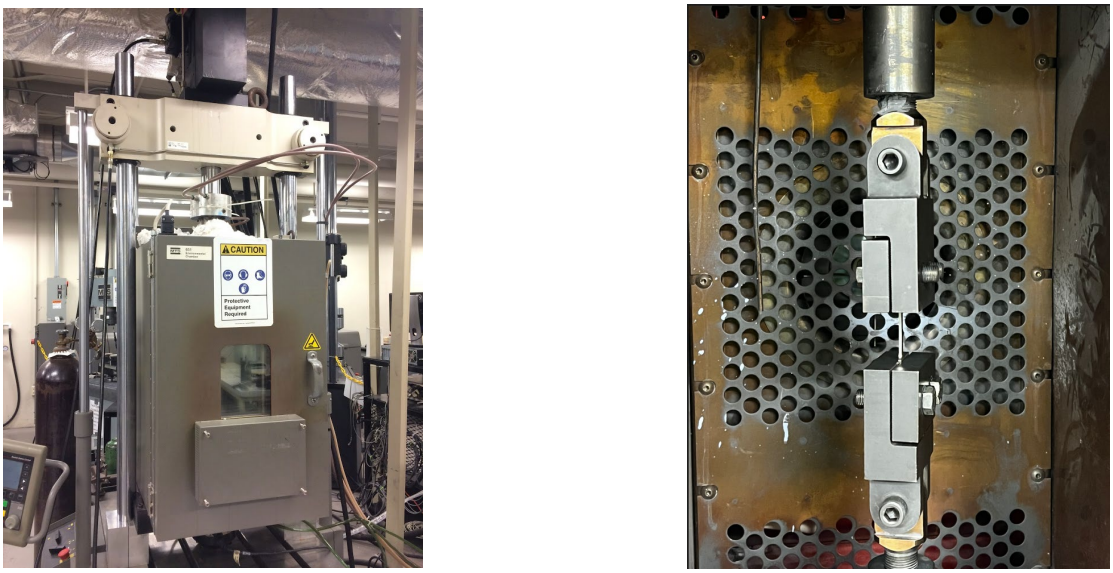

(a) (b)

Figure 2. (a) MTS frame with environmental chamber (b) Specimen installed in the environmental chamber

4. Finite Element Model

Numerical modeling method was used to verify the data obtained from the experimental tensile tests. For this purpose, similar experimental conditions were modeled in ABAQUS using dynamic explicit analysis. The JC parameters obtained from the tests were used for the material model in these simulations. A number of 5040 hexagonal elements, C3D8RT type were used in meshing the model. The tensile coupon meshed in ABAQUS with the boundary conditions can be found in Figure 3. The experimental and the FEA model outcomes were compared to verify the JC parameters for the 304L SS steel alloy.

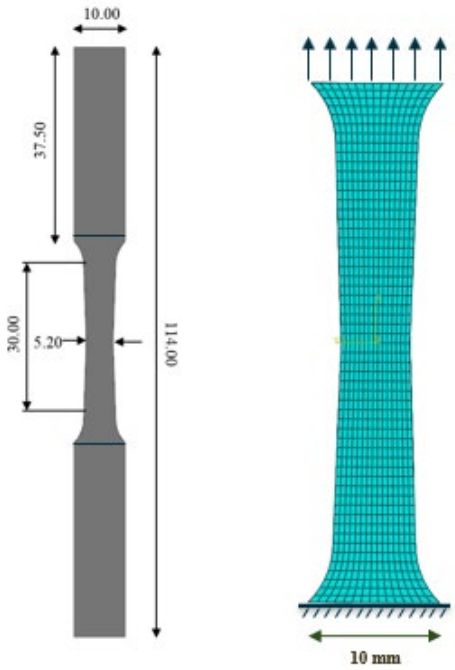

Figure 3. The ASTM-E8 tensile coupon and the meshed tensile coupon in ABAQUS

5. Results and discussion

5.1 Stress-strain curves

From the tensile tests performed at different temperatures and strain rates, the following true stress-strain curves were obtained, in both XY and Z print directions (Figures 4 and 5).

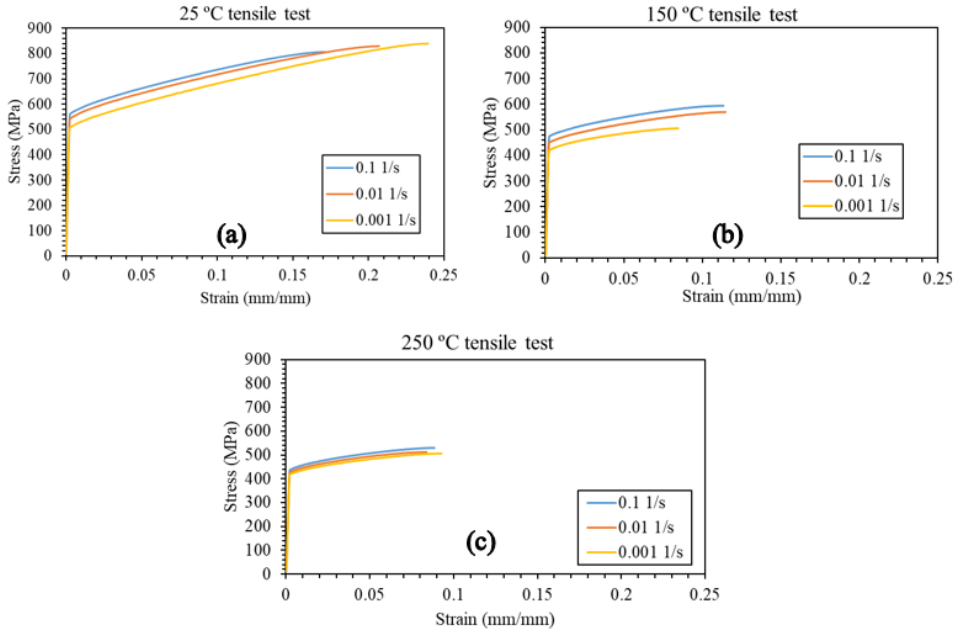

Figure 4. True stress-strain curves in XY-direction (a) at 25ºC (b) 150ºC (c) 250ºC

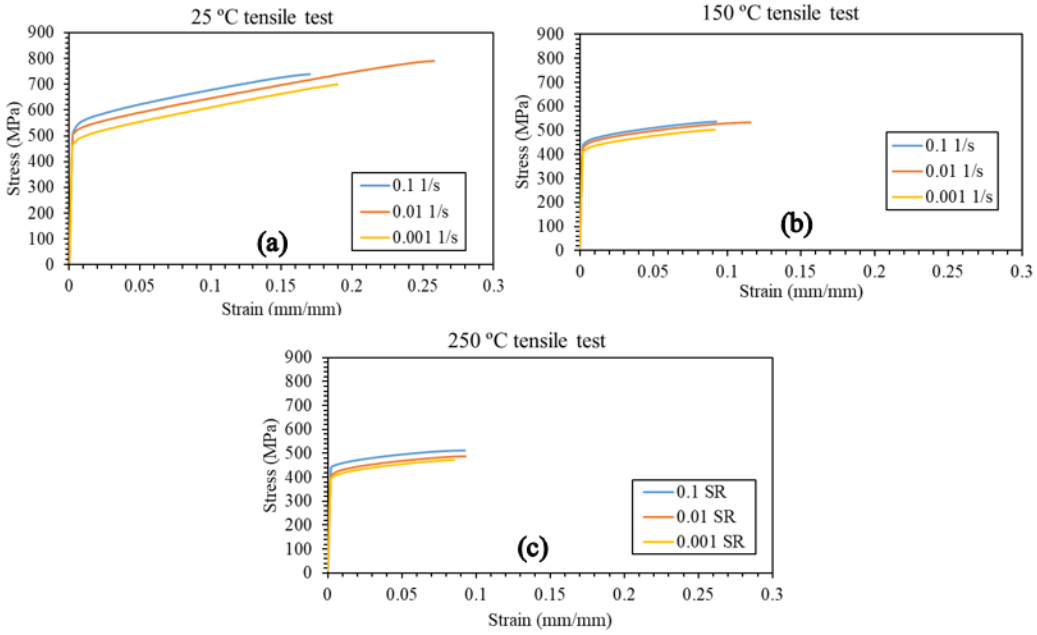

Figure 5. True stress-strain curves in Z-direction (a) at 25ºC (b) 150ºC (c) 250ºC

From the XY stress-strain curves it was evident that the yield stress of the material was highest at 25 ºC with 0.1 s^{-1} strain rate, this was observed to decrease with strain rates to 0.01 s^{-1} and 0.001 s^{-1} at 25 ºC. Similar trend was observed at 150 ºC tests with highest yield stress recorded at 0.1 s^{-1} strain rate followed by 0.01 s^{-1} and 0.001 s^{-1}. The yield stress values dropped significantly for the 250 ºC tests with 0.1 s^{-1} strain rate recording the highest value. For the Z direction testing, the yield stress of the material was highest at 25 ºC with 0.1 s^{-1} strain rate followed by 0.01 s^{-1} and 0.001 s^{-1}. As the temperature increased to 150 ºC and 250 ºC, these values were further reduced. In

comparison between the XY and Z direction tests, the XY specimens recorded highest yield stress values at the respective temperatures and strain rates.

5.2 Johnson-Cook parameters from the tensile tests

A Genetic Algorithm (GA) was written to optimize the experimental data and fit it to the JC material model equation. This code utilizes all the experimental tensile testing data at different temperatures and strain rates to give us the JC parameters as well as fits these values to the equation. Details of the model can be found in Buchely et al. [20]. Thus, the JC model parameters obtained from this study can be found in Tables 3 and 4 for XY and Z direction respectively. The R^2 value of the fitting was higher than 96% which signifies it to be a very good fit to the data. The experimental and the predicted values fit can be found in Figures 6.

Table 4. JC Model parameters for 304L SS in XY build direction

Material	A (MPa)	B (MPa)	n	C	m	$\dot{\varepsilon}_0$ (s^{-1})
304L SS	516.45	812.39	0.7042	0.0117	0.7383	0.001

Table 5. JC Model parameters for 304L SS in Z build direction

Material	A (MPa)	B (MPa)	n	C	m	$\dot{\varepsilon}_0$ (s^{-1})
304L SS	491.83	571.40	0.6422	0.0118	0.7727	0.001

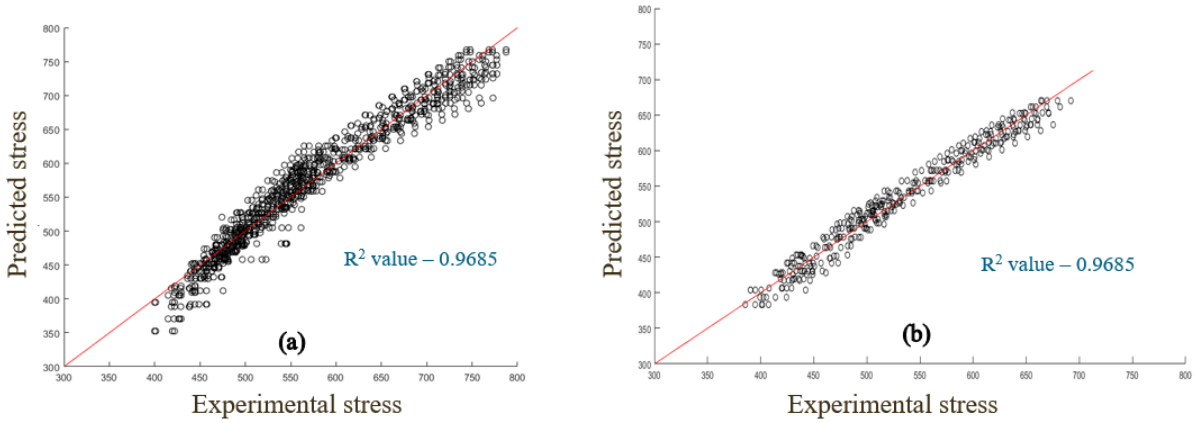

Figure 6. The experimental vs predicted values from the GA model for (a) XY direction (b) Z direction

5.3 Comparison of experimental and modeling results

Figure 7 shows the dimensions of necking region at failure from experiments at 25 ºC for XY direction specimen and it is compared to FE model. It is observed that the strain at failure in FE model is same as that of experiment (Figure 4). Figure 8 shows the comparison of the experimental

and modeling results for the XY and Z direction specimens at 25 ºC. The predicted yield stress for both XY and Z FE models was less than 10 percent when compared to experiment.

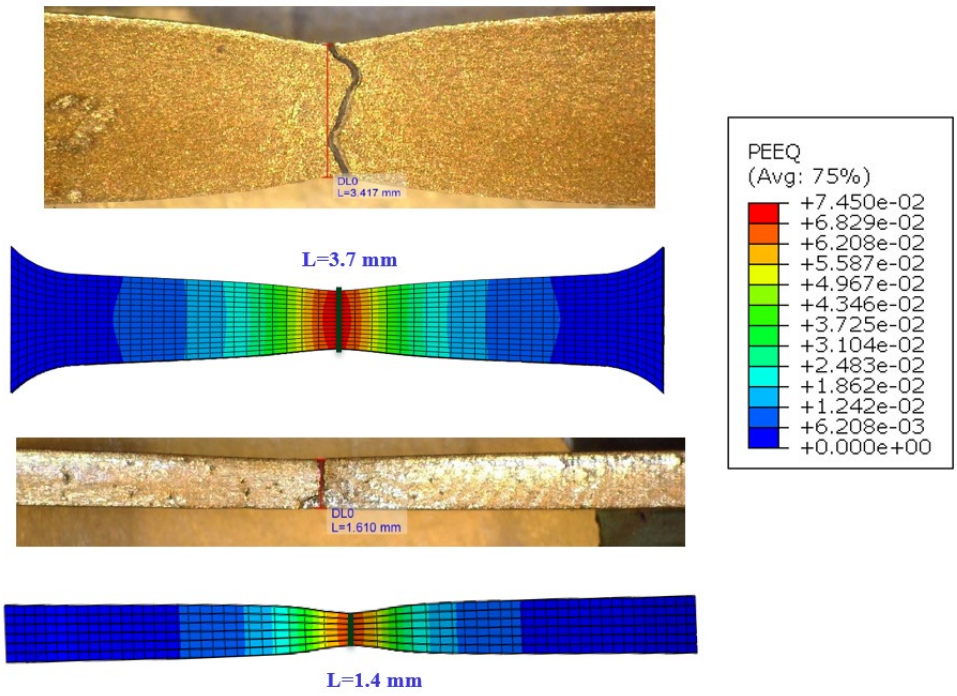

Figure 7. The experimental vs modeling comparison of XY direction specimen at 25 ºC

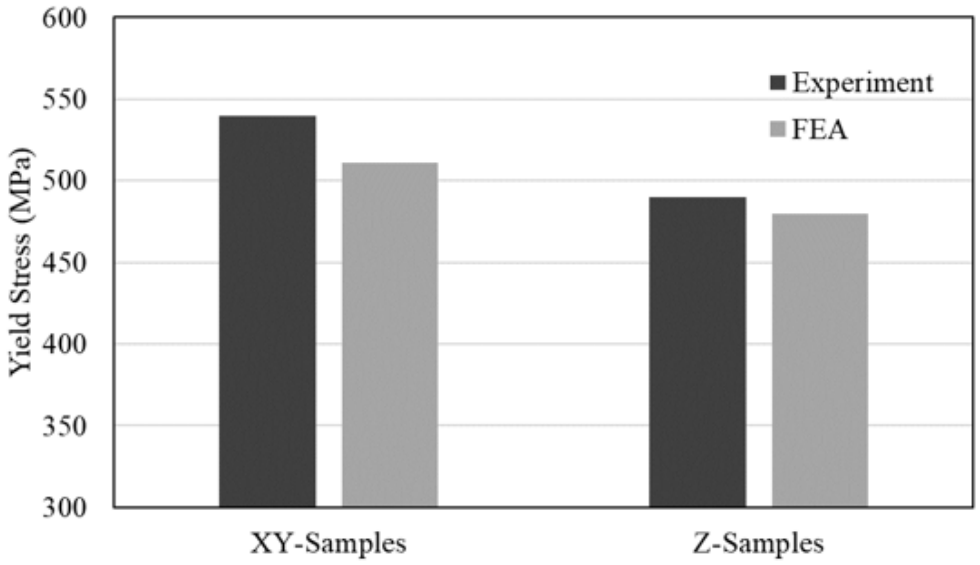

Figure 8. The comparison of the experimental and modeling results of XY and Z direction samples at 25 ºC

6. Conclusions

In summary, 304L stainless steel was used to additively manufacture the tensile coupons. From tensile tests at different temperatures and strain rates, a constitutive JC material model was calibrated using genetic algorithm. The obtained JC parameters were used in developing an FEA model to simulate the experimental tensile tests. This model was used to compare the experimental results and modeling results of the tensile tests to verify the developed material model. The difference in the FEA model results and the experimental results was within 10% error.

References:

1. S. Gorsse, C. Hutchinson, M. Gouné, and R. Banerjee, "Additive manufacturing of metals: A brief review of the characteristic microstructures and properties of steels, Ti-6Al-4V and high-entropy alloys," *Science and Technology of Advanced Materials*, Volume 18, Pages 584-610, 2017.

2. Y. Zhai, D.A. Lados, and J.L. LaGoy, "Additive manufacturing: making imagination the major limitation," *The Journal of The Minerals, Metals & Materials Society*, Volume 66 Pages 808-816, 2014.

3. E. Liverani, S. Toschi, L. Ceschini, and A. Fortunato, "Effect of selective laser melting (SLM) process parameters on microstructure and mechanical properties of 316L austenitic stainless steel," *Journal of Materials Processing Technology*, Volume 249, Pages 255-263, 2017.

4. Z. Sun, X. Tan, S.B. Tor, and W.Y. Yeong, "Selective laser melting of stainless steel 316L with low porosity and high build rates," *Materials & Design*, Volume 104, Pages 197-204, 2016.

5. T. Kurzynowski, K. Gruber, W. Stopyra, B. Kuźnicka, and E. Chlebus, "Correlation between process parameters, microstructure and properties of 316 L stainless steel processed by selective laser melting," *Materials Science and Engineering: A*, Volume 718, Pages 64-73, 2018.

6. F. Calignano, D. Manfredi, E.P. Ambrosio, S. Biamino, M. Pavese, and P. Fino, "Direct fabrication of joints based on direct metal laser sintering in aluminum and titanium alloys," *Procedia CIRP*, Volume 21, Pages 129-132, 2014.

7. J.H. Martin, B.D. Yahata, J.M. Hundley, J.A. Mayer, T.A. Schaedler, and T.M. Pollock, "3D printing of high-strength aluminium alloys," *Nature*, Volume 549, Pages 365-369, 2017.

8. A.A. Popovich, V. S. Sufiiarov, E. V. Borisov, I. A. Polozov, D. V. Masaylo, and A. V. Grigoriev, “Anisotropy of mechanical properties of products manufactured using selective laser melting of powdered materials,” *Russian Journal of Non-Ferrous Metals*, Volume 58, Pages 389–395, 2017.

9. G. Miranda, S. Faria, F. Bartolomeu, E. Pinto, S. Madeira, A. Mateus, P. Carreira, N. Alves, F. S. Silva, and O. Carvalho, “Predictive models for physical and mechanical properties of 316L stainless steel produced by selective laser melting,” *Material Science and Engineering*, Volume 657, Pages 43–56, 2016.

10. C. O. Rios, T. L. Amine, and J. W. Newkirk, “Tensile behavior in selective laser melting,” *International Journal of Advanced Manufacturing Technology*, Volume 96, Pages 1187–1194, 2018.

11. K. Guan, Z. Wang, M. Gao, X. Li, and X. Zeng, “Effects of processing parameters on tensile properties of selective laser melted 304 stainless steel,” *Materials and Design*, Volume 50, Pages 581–586, 2013.

12. S. Haeri, Y. Wang, O. Ghita, and J. Sun, “Discrete element simulation and experimental study of powder spreading process in additive manufacturing,” *Powder Technology*, Volume 306, Pages 45-54, 2017.

13. K. Zhang, T. Liu, W. Liao, C. Zhang, Y. Zheng, and H. Shao, “Simulation of the thermal behavior and analysis of solidification process during selective laser melting of alumina,” In Proceedings of the 29th Annual International Solid Freeform Fabrication Symposium, Austin, TX, USA, 13–15 August, Pages 1808–1820, 2018.

14. E. Zaretsky E, A. Stern A, N. Frage, “Dynamic response of AlSi10Mg alloy fabricated by selective laser melting,” *Material Science and Engineering: A*, Volume 688, Pages 364-370, 2017.

15. A. Shrot, and M. Baker, “Determination of Johnson-Cook parameters from machining simulation,” *Computational Material Science*, Volume 52, Pages 298-304, 2012.

16. J. Kadkhodapour, H. Montazerian, A.Ch. Darabi, A.P. Anaraki, S.M. Ahmadi, A.A. Zadpoor, and S. Schmauder, “Failure mechanisms of additively manufactured porous biomaterials: Effects of porosity and type of unit cell,” *Journal of the Mechanical Behavior of Biomedical Materials*, Volume 50, Pages 180-191, 2015.

17. O. Fashanu, M. F. Buchely, M. Spratt, J. Newkirk, K. Chandrashekhara, H. Misak, and M. Walker, "Effect of SLM Build Parameters on the Compressive Properties of 304L Stainless Steel," *Journal of Manufacturing and Materials Processing*, Volume 3, 2019.

18. E. Liverani, S. Toschi, L. Ceschini, and A. Fortunato, “Effect of selective laser melting (SLM) process parameters on microstructure and mechanical properties of 316L austenitic

stainless steel," *Journal of Materials Processing Technology*, Volume 249, Pages 255-263, 2017.

19. S. Ganguly, X. Wang, K. Chandrashekhara, M. F. Buchely, S. Lekakh, R. J. O'Malley, A. Kumar,and V. Thapliyal," Modeling and simulation of mass flow during hot rolling low carbon steel I-beam," *Journal of Manufacturing Processes*, Volume 64, Pages 285-293, 2021.

20. M.F Buchely, X. Wang, D. C. Van Aken, R. J. O'Malley, S. Lekakh, and K. Chandrashekhara, "The use of genetic algorithms to calibrate Johnson–Cook strength and failure parameters of AISI/SAE 1018 Steel, *"Journal of Engineering Materials and Technology (ASME)*, Volume 141, Pages 021012, 2019.